

## Femtosecond laser-drilled capillary integrated into a microfluidic device

Tyson N. Kim, Kyle Campbell, Alex Groisman, David Kleinfeld, and Chris B. Schaffer<sup>a)</sup>  
*Department of Physics, University of California, San Diego, La Jolla, California 92093*

(Received 17 November 2004; accepted 28 March 2005; published online 10 May 2005)

Recent growth in microfluidic technology is, to a large extent, driven by soft lithography, a high-throughput fabrication technique where polymer materials, such as poly(dimethyl) siloxane (PDMS), are molded to form microscopic channel networks. Nevertheless, the channel architectures that can be obtained by molding are limited. We address this limitation by using femtosecond laser micromachining to add unmoldable features to the microfluidic devices. We apply laser ablation to drill microcapillaries, with diameters as small as 0.5  $\mu\text{m}$  and aspect ratios as high as 800:1, in the walls of molded PDMS channels. Finally, we use a laser-drilled microcapillary to trap a polystyrene bead by suction and hold it against a shear flow. © 2005 American Institute of Physics.  
[DOI: 10.1063/1.1926423]

The use of microfluidic devices has grown rapidly in recent years, due, in large part, to the introduction of soft-lithography.<sup>1</sup> In this method, a microfluidic device is cast from a polymer material using a photolithographically produced master mold of the desired channel network. One of the most commonly used polymers is poly(dimethyl) siloxane (PDMS), a chemically inert, optically transparent silicon elastomer.<sup>2</sup> Because soft lithography is based on molding, the channel networks are inherently limited to two-dimensional arrangements. This limitation has been partially addressed by using master molds with multilevel relief<sup>3</sup> and by stacking multiple two-dimensional PDMS slabs.<sup>4–6</sup> The former method, however, is not truly three-dimensional (3D), and the latter method is tedious and cannot achieve micrometer precision. In addition, several commonly used devices, such as a tapered glass microcapillary, are difficult to emulate using soft-lithography. Overcoming the limitation to two-dimensional networks and enabling the fabrication of a broader range of devices will significantly enhance microfluidic technology, opening the door to new applications.

Femtosecond laser pulses provide a unique micromachining tool that allows the surface or bulk of a transparent material to be modified with micrometer precision. A tightly focused femtosecond laser pulse can deposit energy into a transparent material through high-order nonlinear absorption,<sup>7,8</sup> producing 3D-localized material ablation either on the surface,<sup>9</sup> or in the bulk.<sup>10,11</sup> By translating the laser focus from a surface into the bulk of the sample, a capillary can be drilled using this laser ablation. Recently, this technique was used to create 2- $\mu\text{m}$  diameter capillaries in fused silica.<sup>12</sup> One of the key issues in drilling high aspect-ratio capillaries is the efficient removal of debris to prevent clogging. In previous work, debris was removed by water that wicked into the capillaries during drilling.<sup>12–14</sup> Although this direct laser writing has high precision and 3D capability, it is inherently low throughput and is impractical for machining entire networks that may only require high precision and 3D elements in small selected areas.

In this article, we demonstrate the machining of microcapillaries in the walls of molded PDMS channels by femtosecond laser ablation. We take advantage of the best qualities

of both soft lithography and femtosecond laser micromachining by molding channel networks with high throughput and using laser drilling to add small, high precision elements that, because of their location, cannot be obtained by molding.

The first part of our fabrication process for microfluidic devices follows common soft-lithography protocol.<sup>1,2</sup> A photomask with multiple copies of a desired channel network is printed with 4000 dot-per-inch resolution. A master mold is made by spin coating a 40- $\mu\text{m}$  thick layer of photocurable epoxy (SU8-2050, MicroChem, Newton, MA) onto a silicon wafer, exposing the wafer to UV light through the photomask, and developing the epoxy. A 5-mm thick cast of PDMS (Sylgard 184, Dow Corning, Midland, MI) is made using the wafer as a mold, and the cast is cut into individual devices. Next, holes to feed liquids into the channels are punched in the devices with a luer stub, and the devices are soaked for 1 h in 0.01-M HCl at 80 °C to make their surface more hydrophilic. Finally, to close the channels, a glass cover slip is bonded to the open face of each device by overnight baking at 80 °C.

Capillaries are machined in a molded device using a 100-fs duration, 800-nm wavelength, 1-kHz repetition rate train of pulses that is attenuated using neutral density filters and is shutter controlled. The pulses are focused into the microfluidic device using a high numerical aperture (NA) microscope objective and the device is translated relative to the laser focus using computer-controlled translation stages. The focus is first located in a molded channel filled with ethanol [Fig. 1(a)] and then moved through the channel walls into the bulk of the PDMS, drilling a microcapillary [Fig. 1(b)]. This procedure allows for the formation of 3D microcapillaries that are not adjacent to the face of the PDMS device and cannot be created by molding. During drilling, there is a flow of ethanol in the molded channels that carries away the debris formed by laser ablation of the PDMS. Ethanol is chosen because it wicks rapidly in PDMS, has a refractive index of 1.37 close to that of PDMS (1.41), and induces relatively little swelling in PDMS.<sup>15</sup> Note that in the absence of ethanol, the opening of a laser-drilled microcapillary becomes clogged with debris after drilling only a few micrometers. After the laser-drilled microcapillary is complete, it is flushed with a solution of 0.5% (wt/vol) HF in ethanol for five minutes and then washed with pure ethanol [Fig. 1(c)]. The HF treatment stabilizes even the smallest

<sup>a)</sup> Author to whom correspondence should be addressed; electronic mail: cschaffer@ucsd.edu

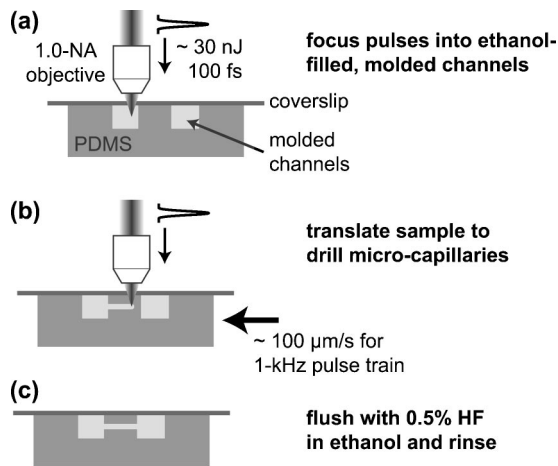


FIG. 1. Femtosecond laser drilling of microcapillaries in PDMS.

microcapillaries, allowing long-term flow of ethanol or water ( $>24$  h) and dry storage ( $>1$  week). Without HF treatment, laser-drilled capillaries with a diameter smaller than  $5$   $\mu\text{m}$  are observed to clog within an hour. The HF treatment did not cause any visible change in the size or shape of the capillaries.

We optimized the machining parameters in PDMS by drilling capillaries with different laser energies, sample translation rates, and focusing conditions [Fig. 2]. To image the drilling *in situ*, we fill the device with a solution of 10-mM fluorescein in ethanol and use two-photon laser scanning microscopy (TPLSM).<sup>16</sup> Two-photon imaging is carried out on a home-built microscope<sup>17</sup> utilizing a 100-fs duration, 800-nm wavelength, 76-MHz repetition rate train of laser pulses. Pixel integration times are about  $2$   $\mu\text{s}$ , and the laser pulse energy is  $10$  pJ. Capillaries are drilled either by alternately translating the sample and firing a group of pulses (move and fire) or by irradiating with a 1-kHz pulse train while continuously moving (smooth translation). Sample translation is either perpendicular to (transverse) or along (axial) the incident direction of the laser beam. We use 1.0-NA water-immersion and 1.4-NA oil-immersion focusing optics and find the threshold energy for capillary formation to be  $15$  and  $10$  nJ at the laser focus, respectively. The cleanest capillary profiles are achieved with smooth translation at around  $100$   $\mu\text{m/s}$  over a wide range of laser energies (data not shown). For transverse drilling at 1.0 NA with smooth translation, the capillary profile is oval when using near-threshold laser energies, consistent with the shape of the focal volume, and becomes V shaped for higher energies, consistent with previously reported damage profiles in glass<sup>11</sup> [Figs. 2(a) and 2(b)]. For near-threshold energies, the capillaries maintain a constant profile at entrance and exit holes, i.e., there is no flaring of the profile at the ends [Fig. 2(a)]. The capillary shape is highly reproducible as long as the same laser, focusing, and translation parameters are used [Fig. 2(c)]. Capillaries like those in Fig. 2(c) were produced with a length of up to  $2$  mm, corresponding to an aspect ratio of  $\sim 800:1$  (data not shown). The capillary profiles for 1.4-NA focusing with transverse move and fire drilling are similar to those observed with 1.0-NA focusing [Fig. 2(d)]. Capillaries drilled axially, using the move and fire method with 1.0-NA focusing, have round profiles and diameters as small as  $0.5$   $\mu\text{m}$  for near-threshold laser energies [Figs. 2(e) and 2(f)]. Finally, by combining transverse and axial drilling,

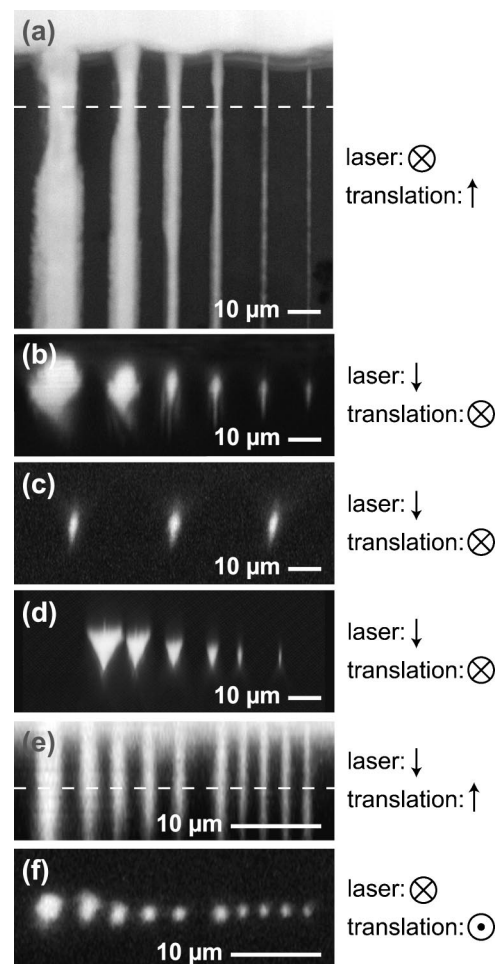


FIG. 2. TPLSM images of microcapillaries drilled in PDMS. The incident direction of the laser and the direction of device translation relative to the laser focus are indicated for each image. (a) Top and (b) cross-sectional views of capillaries drilled  $25$   $\mu\text{m}$  beneath the cover slip with 1.0-NA focusing, transverse translation at  $100$   $\mu\text{m/s}$  with 1-kHz irradiation, and laser energies at the focus of (left to right):  $550$ ,  $270$ ,  $140$ ,  $70$ ,  $34$ , and  $17$  nJ. (c) Capillaries drilled using the same parameters as in (a), but with  $33$  nJ. (d) Capillaries drilled  $20$   $\mu\text{m}$  beneath the cover slip using 1.4-NA focusing, transverse translation in  $1$ - $\mu\text{m}$  steps between bursts of 10 laser pulses ( $0.1$ - $\mu\text{m}$  steps for lowest energy capillary), and energies of (left to right):  $340$ ,  $170$ ,  $90$ ,  $40$ ,  $20$ , and  $10$  nJ. (e) Top and (f) cross-sectional views of capillaries drilled into the floor (starting  $50$   $\mu\text{m}$  beneath the cover slip) of a molded channel using 1.0-NA focusing, axial translation in  $0.2$   $\mu\text{m}$  steps between bursts of 10 pulses, and energies of (left to right)  $790$ ,  $550$ ,  $360$ ,  $230$ ,  $180$ ,  $160$ ,  $140$ ,  $110$ ,  $90$ , and  $70$  nJ. The dashed lines in (a) and (e) indicate the location of the cross sections in (b) and (f), respectively.

we create spiral-shaped, 3D microcapillaries (data not shown). We note that the walls of the laser-drilled capillaries retain the optical transparency of PDMS.

We use scanning electron microscopy (SEM) to view the microcapillary morphology in greater detail. The entrance hole of the laser-drilled microcapillary is exposed by slicing a PDMS device along a molded channel. We coat the sample with a thin layer of gold before imaging. Capillaries drilled transversely with smooth translation, 1.0-NA focusing, and near-threshold laser energies have a size and shape comparable to that of the laser focal volume [Fig. 3(a)]. The internal surface of channels drilled with about twice the threshold energy show  $100$ -nm scale roughness [Fig. 3(b)].

As a demonstration of the utility of our technique, we connect two molded channels with a laser-drilled microcapillary, enabling applications that cannot be realized using only molded networks. Using soft lithography, we mold a

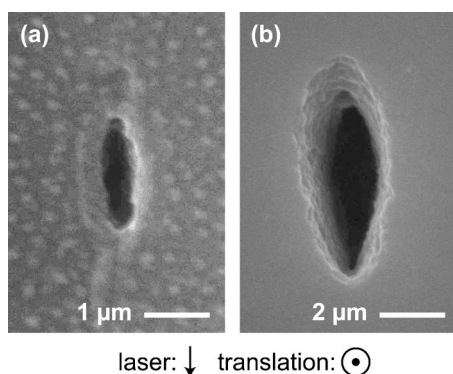


FIG. 3. SEM images of the entrance hole of microcapillaries drilled in PDMS using a 1-kHz, 800-nm, 100-fs pulse train of (a) 17 nJ and (b) 27 nJ energy, 1.0-NA focusing, and transverse translation at 100  $\mu\text{m/s}$ . The speckled appearance of the surface in (a) is a result of a coating artifact.

microfluidic device with two channels, one U shaped and one T shaped, separated by a 35- $\mu\text{m}$  thick wall of PDMS [Fig. 4(a)]. A microcapillary is then drilled through this wall about halfway between the cover slip and the bottom of the 40- $\mu\text{m}$  deep channels using the same parameters as in Fig. 2(c). During drilling there is a flow of ethanol in the U channel, facilitating debris removal. After the device is complete, the pressures applied to the inlet and outlet of the U channel are set to the same value and the difference between this value and the pressure at the T junction controls flow through the microcapillary.

When the pressure in the U channel is higher than that at the T junction, there is flow through the microcapillary into the T channel [Fig. 4(b)]. This flow is visualized by using a solution of fluorescein in ethanol in the U channel and pure ethanol in the T channel. The pressures applied to the sides of the T are equal and are above that at the leg of the T, creating a sheath flow, where the stream of fluorescent ethanol from the micro-capillary is squeezed by two streams of nonfluorescent ethanol from the sides of the T. The flow pattern in Fig. 4(b) was stable for longer than 24 h.

Applying suction to the microcapillary provides a means to trap a particle at the stagnation point of an extensional flow [Fig. 4(c)] or in a high-shear flow [Fig. 4(d)]. The pressure applied to the U channel is lower than at the T junction by about 40 kPa. The T channel is filled with a suspension of 4.6- $\mu\text{m}$  diameter fluorescent polystyrene beads in a solution of 13.5% (wt/vol) NaCl in water (for neutral buoyancy of the beads). One of the beads is held at the capillary opening by the pressure difference (suction) between the T side and the U side of the microcapillary. Other beads follow the flow and produce streaks. In Fig. 4(c), the flow in the T channel is from the sides and down the leg of the T [as in Fig. 4(b)], while in Fig. 4(d) the port at the leg of the T is blocked and a flow between the two sides of the T is generated by applying different pressures to them. In the latter case, the bead remains trapped up to the flow rate of about 100 mm/s (as measured by the streaks near the center) corresponding to a shear rate of about 8000  $\text{s}^{-1}$  near the wall and a longitudinal drag force of about 700 pN acting on the bead.

In conclusion, we use tightly focused femtosecond laser pulses to drill small diameter, high aspect-ratio microcapillaries in molded PDMS microfluidic devices. This technique allows the fabrication of a wider range of channel architectures than molding alone and will enable new microfluidic applications. For example, the microfluidic network with an

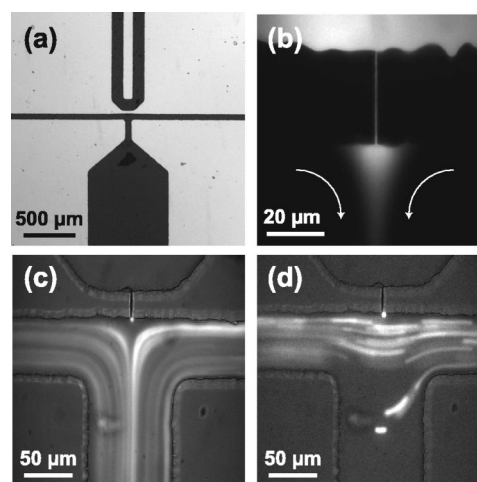


FIG. 4. Molded microfluidic device with an integrated, laser-drilled microcapillary. (a) Device overview showing U shaped (above) and T shaped (below) channels, filled with black ink for contrast. (b) TPLSM image of flow of fluorescent solution through the microcapillary that connects the U and T channels. The white arrows indicate the direction of flow in the T channel. (c) and (d) Wide-field fluorescence images of a 4.6- $\mu\text{m}$  diameter fluorescent bead trapped by suction at the opening of the microcapillary. Streaks in the T channel are formed by other beads that follow the flow. The exposure times in (c) and (d) is 4 and 1 ms, respectively.

integrated microcapillary shown in Fig. 4 could be used to trap individual living cells and expose them to different physical and chemical environments by controlling flow through the molded channels.

The authors thank H.-C. Kim and S. Fainman for help acquiring SEM images. This work was funded by the NSF REU program (TNK), NSF Grant No. MCB-0331306 (AG), the David and Lucille Packard Foundation (DK), and the La Jolla Interfaces in Science program (CBS).

- <sup>1</sup>Y. N. Xia and G. M. Whitesides, *Annu. Rev. Mater. Sci.* **28**, 153 (1998).
- <sup>2</sup>J. C. McDonald and G. M. Whitesides, *Acc. Chem. Res.* **35**, 491 (2002).
- <sup>3</sup>A. D. Stroock, S. K. Dertinger, A. Ajdari, I. Mezic, H. A. Stone, and G. M. Whitesides, *Science* **295**, 647 (2002).
- <sup>4</sup>H. K. Wu, T. W. Odom, D. T. Chiu, and G. M. Whitesides, *J. Am. Chem. Soc.* **125**, 554 (2003).
- <sup>5</sup>B. H. Jo, L. M. Van Lerberghe, K. M. Motsegood, and D. J. Beebe, *J. Microelectromech. Syst.* **9**, 76 (2000).
- <sup>6</sup>J. R. Anderson, D. T. Chiu, R. J. Jackman, O. Cherniavskaya, J. C. McDonald, H. K. Wu, S. H. Whitesides, and G. M. Whitesides, *Anal. Chem.* **72**, 3158 (2000).
- <sup>7</sup>B. C. Stuart, M. D. Feit, S. Herman, A. M. Rubenchik, B. W. Shore, and M. D. Perry, *Phys. Rev. B* **53**, 1749 (1996).
- <sup>8</sup>C. B. Schaffer, A. Brodeur, and E. Mazur, *Meas. Sci. Technol.* **12**, 1784 (2001).
- <sup>9</sup>A. P. Joglekar, H. H. Liu, E. Meyhofer, G. Mourou, and A. J. Hunt, *Proc. Natl. Acad. Sci. U.S.A.* **101**, 5856 (2004).
- <sup>10</sup>E. N. Glezer, M. Milosavljevic, L. Huang, R. J. Finlay, T. H. Her, J. P. Callan, and E. Mazur, *Opt. Lett.* **21**, 2023 (1996).
- <sup>11</sup>C. B. Schaffer, A. O. Jamison, and E. Mazur, *Appl. Phys. Lett.* **84**, 1441 (2004).
- <sup>12</sup>Y. Iga, T. Ishizuka, W. Watanabe, K. Itoh, Y. Li, and J. Nishii, *Jpn. J. Appl. Phys., Part 1* **43**, 4207 (2004).
- <sup>13</sup>Y. Li, K. Itoh, W. Watanabe, K. Yamada, D. Kuroda, J. Nishii, and Y. Y. Jiang, *Opt. Lett.* **26**, 1912 (2001).
- <sup>14</sup>M. S. Giridhar, K. Seong, A. Schulzgen, P. Khulbe, N. Peyghambarian, and M. Mansuripur, *Appl. Opt.* **43**, 4584 (2004).
- <sup>15</sup>J. N. Lee, C. Park, and G. M. Whitesides, *Anal. Chem.* **75**, 6544 (2003).
- <sup>16</sup>W. R. Zipfel, R. M. Williams, and W. W. Webb, *Nat. Biotechnol.* **21**, 1369 (2003).
- <sup>17</sup>P. S. Tsai, N. Nishimura, E. J. Yoder, E. M. Dolnick, G. A. White, and D. Kleinfeld, in *In Vivo Optical Imaging of Brain Function*, edited by R. D. Frostig (CRC Press, Boca Raton, 2002), pp. 113.